

Type 1 AGN at low z

J Stern and A Laor

Department of Physics, Technion – Israel Institute of Technology, Haifa, Israel

E-mail: stern@physics.technion.ac.il, laor@physics.technion.ac.il

Abstract. We present the emission properties of a sample of 3579 type 1 AGN, selected based on the detection of broad H α emission. The sample covers the range of black hole mass $10^6 < M_{\text{BH}}/M_{\odot} < 10^{9.5}$ and luminosity in Eddington units $10^{-3} < L/L_{\text{Edd}} < 1$. Our main results are: 1. The distribution of the H α FWHM values is independent of luminosity. 2. The observed mean optical-UV SED is well matched by a fixed shape SED of luminous quasars, which scales linearly with broad H α luminosity, and a host galaxy contribution. 3. The host galaxy r -band (fibre) luminosity function follows well the luminosity function of inactive non-emission line galaxies (NEG), consistent with a fixed fraction of $\sim 3\%$ of NEG hosting an AGN, regardless of the host luminosity. 4. The optical-UV SED of the more luminous AGN shows a small dispersion, consistent with dust reddening of a blue SED, as expected for thermal thin accretion disc emission. 5. There is a rather tight relation of $\nu L_{\nu}(2 \text{ keV})$ and broad H α luminosity, which provides a useful probe for unobscured (true) type 2 AGN.

1. Introduction

We examine the emission properties of a new sample of low z broad line AGN, aimed to be an extension of the SDSS quasar catalog (QCV, Schneider et al. 2010) to low luminosities. This contribution summarizes the main results obtained on the distribution of the broad line FWHM (§3), the host galaxies (§4), and the AGN spectral energy distribution (§§5–7). Full details of the methods used, and a discussion of the implication of the results, are given in the main article (Stern & Laor, accepted).

2. Sample Creation

The type 1 (T1) sample is selected from the SDSS 7th data release (DR7, Abazajian et al. 2009), based on the detection of a broad H α emission line. The parent sample includes 232 837 spectra with $S/N > 10$ and $0.005 < z < 0.31$. The broad H α emission is identified by modeling the nearby narrow emission lines, stellar absorption features and featureless continuum. We find broad H α emission in 3 579 objects (1.5%), which constitute the T1 sample.

The optical spectra in the T1 sample are supplemented by nearly complete near IR photometry from 2MASS (Skrutskie et al. 2006, detection rate 97%) and UV photometry from GALEX (Martin et al. 2005, 93%). We also add X-ray photometry from the ROSAT (Voges et al. 1999) survey, available for 43% of the T1 objects. The measured broad H α luminosities ($L_{\text{bH}\alpha}$) and FWHMs (Δv) and the photometric luminosities are available electronically.

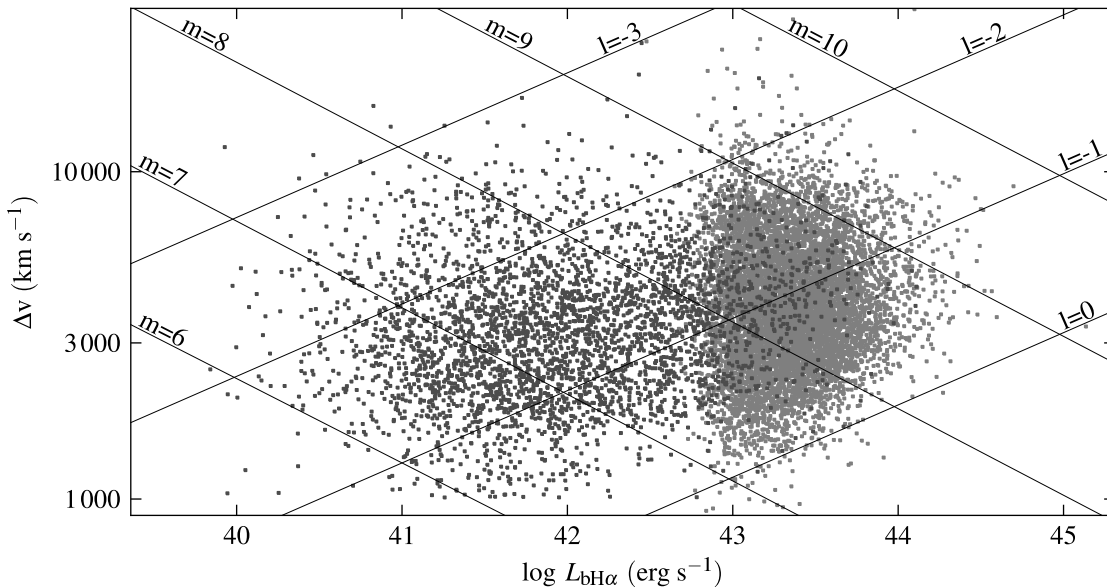


Figure 1. The distributions of the T1 (dark gray) and QCIV (light gray) samples in the broad H α luminosity vs. FWHM plane. Crossing lines mark decades of the implied M_{BH} and L/L_{Edd} .

3. How broad do the broad lines get?

Various theoretical models of the broad line region (BLR) and the AGN ionizing continuum predict an upper limit on Δv , beyond which the BLR does not exist (Nicastro 2000, Elitzur and Shlosman 2006, Laor & Davis 2011). The models differ in the dependence of the maximal Δv on luminosity. In Figure 1, we plot the $L_{\text{bH}\alpha}$ vs. Δv distributions of the T1 objects and the 8185 QCIV objects where the broad H β is available (measurements from Shen et al. 2008).

The T1 sample extends down by two orders of magnitude in $L_{\text{bH}\alpha}$ compared to QCIV. The Eddington ratio L/L_{Edd} ($\equiv 10^l$) and black hole mass M_{BH} ($\equiv 10^m M_{\odot}$) are derived from $L_{\text{bH}\alpha}$ and Δv , in a manner similar to Greene & Ho (2005). It can be seen that the Eddington limit ($l = 0$) sets a minimum Δv with increasing $L_{\text{bH}\alpha}$ for $L_{\text{bH}\alpha} > 10^{42.5}$ erg s $^{-1}$. This, together with the rarity of AGN with $m > 9.5$, leads to a decrease in the range of observed Δv values with increasing $L_{\text{bH}\alpha}$. A similar convergence of the range of Δv for the Mg II and C IV lines at the highest continuum luminosities was noted by Fine et al. (2008, 2010).

There is a steep decline in the number of objects with $\Delta v > 10\,000$ km s $^{-1}$, at all luminosities. This decline is seen clearly in Figure 2, which plots the Δv distribution of the combined T1 + QCIV sample at different L_{bol} . The distributions are remarkably similar, showing a roughly linear decline of $\log(dN/d \log \Delta v)$ vs. Δv , or equivalently $dN/d \log \Delta v \propto e^{-\Delta v/\Delta v_0}$, with $\Delta v_0 \approx 2700$ km s $^{-1}$. The origin of this similarity is not clear, as the Δv distributions should be set by the distribution of the m and l values. Either these distributions somehow lead to a Δv distribution which is independent of $L_{\text{bH}\alpha}$, or it may imply that Δv , rather than m and l , sets the observed Δv distribution through some unknown mechanism. Note the effect of the Eddington limit at $\Delta v < 3000$ km s $^{-1}$, which increases the minimal Δv and the peak position with increasing L_{bol} .

4. How does the AGN fraction change with galaxy luminosity?

Kauffmann et al. (2003), and various follow up studies, found that AGN tend to reside in massive hosts. We therefore examine the T1 fraction as a function of host luminosity.

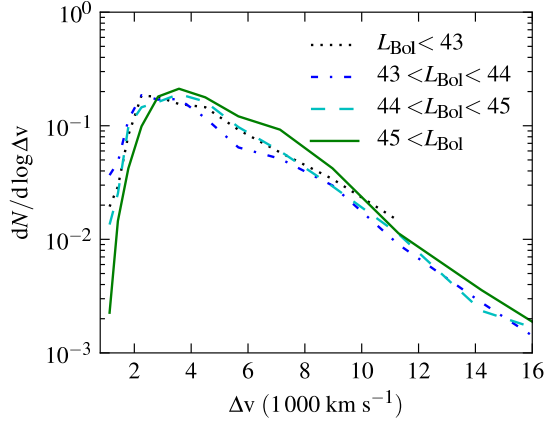


Figure 2. The FWHM distribution of the T1+QCIV sample, at different L_{bol} bins.

Figure 3. The spectral type distribution of galaxies in the parent sample, as a function of luminosity (r band). Non-T1 classifications are from Brinchmann et al. (2004). The ‘T1 host’ line is corrected for the AGN contribution. The lower panel shows the number of objects per 0.25 decade in νL_ν .

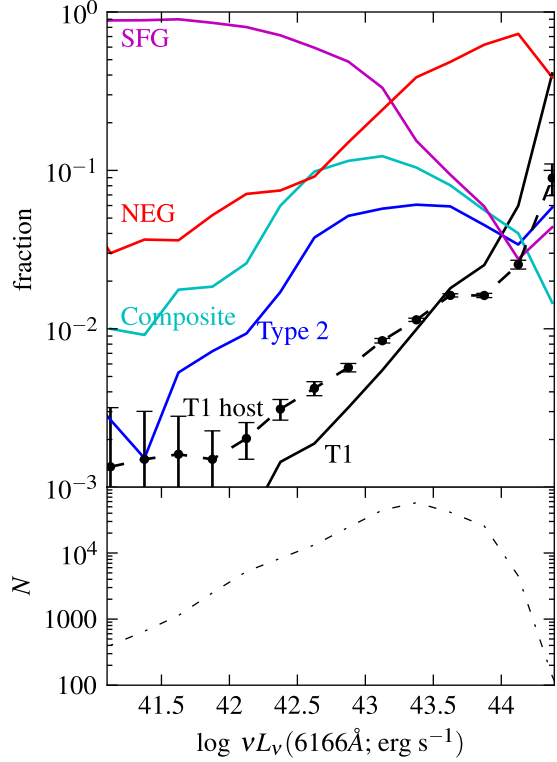


Figure 3 presents the classification of $z < 0.2$ galaxies in the parent sample (§2) as a function of the spectroscopically measured $\nu L_\nu(6166\text{\AA})$. The type 2, Star Forming Galaxy (SFG), Non-Emission line Galaxy (NEG) and composite classifications (based on the equivalent width and BPT ratios of the narrow lines) are taken from Brinchmann et al (2004). At low luminosities $>90\%$ of the SDSS galaxies are SFG, while at high luminosities the NEG dominate. The ‘T1 host’ line is derived from the $\nu L_\nu(6166\text{\AA})$ of the T1 objects, corrected for the AGN contribution (see §5 below). Remarkably, the T1 host fraction follows well the NEG fraction, or equivalently, their galaxy luminosity distribution is similar. This may suggest that T1s reside in NEG, as also implied by their similar concentration indices and bulge/total light ratios (Kauffmann et al. 2003). The fraction of NEG hosting broad line AGN at the level detectable in this study is $\sim 3\%$, independent of galaxy luminosity.

5. How does the AGN spectral energy distribution (SED) depend on luminosity?

Figure 4 compares $L_{\text{bH}\alpha}$ with the observed $2.2 \mu\text{m} - 2 \text{keV}$ continuum luminosity, in the T1 sample. In the luminous bins in the FUV, NUV and 3940\AA panels, the slopes are consistent with a linear relation, in all other bands and luminosities the slopes are flatter. Since the FUV occurs close to the peak position of the AGN SED (e.g. Zheng et al. 1997), the linear relation between $\nu L_\nu(\text{FUV})$ and $L_{\text{bH}\alpha}$ suggests that $L_{\text{bH}\alpha}$ provides a good estimator of L_{bol} . Also, the linear relation suggests that the mean covering factor of the BLR is independent of luminosity.

In all bands excluding X-ray, there is a transition from a steeper slope to a flatter slope with decreasing $L_{\text{bH}\alpha}$. The transition $L_{\text{bH}\alpha}$ increases with wavelength, up to a maximum of $\simeq 10^{43} \text{ erg s}^{-1}$ at $1.2\mu\text{m}$. The transition occurs due to the host contribution, which peaks at $1.2\mu\text{m}$.

The transition between AGN and host dominance of the SED can be seen in Figure 5. The left panel plots the mean SEDs in the $L_{\text{bH}\alpha}$ bins, i.e. each line connects the mean values of

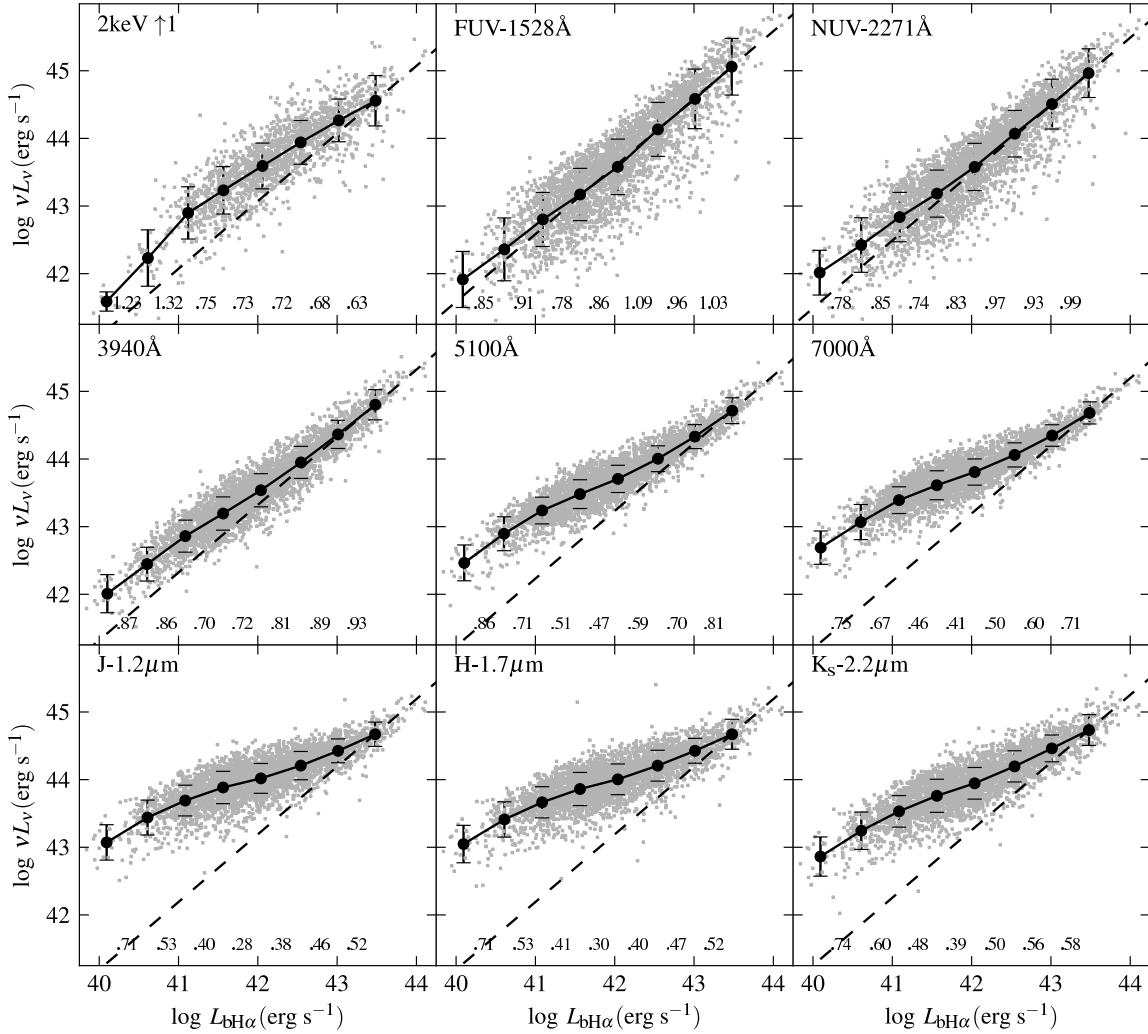


Figure 4. The $L_{bH\alpha}$ vs. observed (AGN+host) νL_ν from the X-ray to the NIR, in the T1 sample. The X-ray νL_ν are shifted upward by 1 decade for presentation purpose. The large black dots and associated error bars mark the mean and dispersion of νL_ν in half-decade wide $L_{bH\alpha}$ bins. The solid lines connect the means of adjacent bins, with the local slopes written underneath. Dashed lines depict a linear relation, normalized to the highest $L_{bH\alpha}$ bin.

different continuum wavelengths for the same $L_{bH\alpha}$ (Fig. 4). Note the transition from an AGN-dominated UV peaked SED to a galaxy-dominated NIR peaked SED with decreasing $L_{bH\alpha}$. As the net AGN SED, we take the Richards et al. (2006, hereafter R06) SED derived from luminous quasars in the SDSS. We scale the R06 SED to the UV in the highest $L_{bH\alpha}$ bin, and rescale by the relative $L_{bH\alpha}$ of the lower seven bins. The scaled R06 SEDs are the putative net AGN SEDs, assuming the mean SED remains fixed with luminosity and scales linearly with $L_{bH\alpha}$. In the middle panel of Fig. 5 we plot the residuals derived by subtracting the AGN from the observed SED, and in the right panel we plot the mean SEDs of inactive SDSS galaxies, with z -distributions matched to the z -distributions of each $L_{bH\alpha}$ bin.

The residuals all appear to have a typical galaxy SED. This justifies (qualitatively) the simple scaling prescription we used for the net AGN SED. Note the significant excess luminosity in the K_s and H bands in the most luminous residuals, and the non-linear $\nu L_\nu(\text{X-ray})$ - $L_{bH\alpha}$ relation

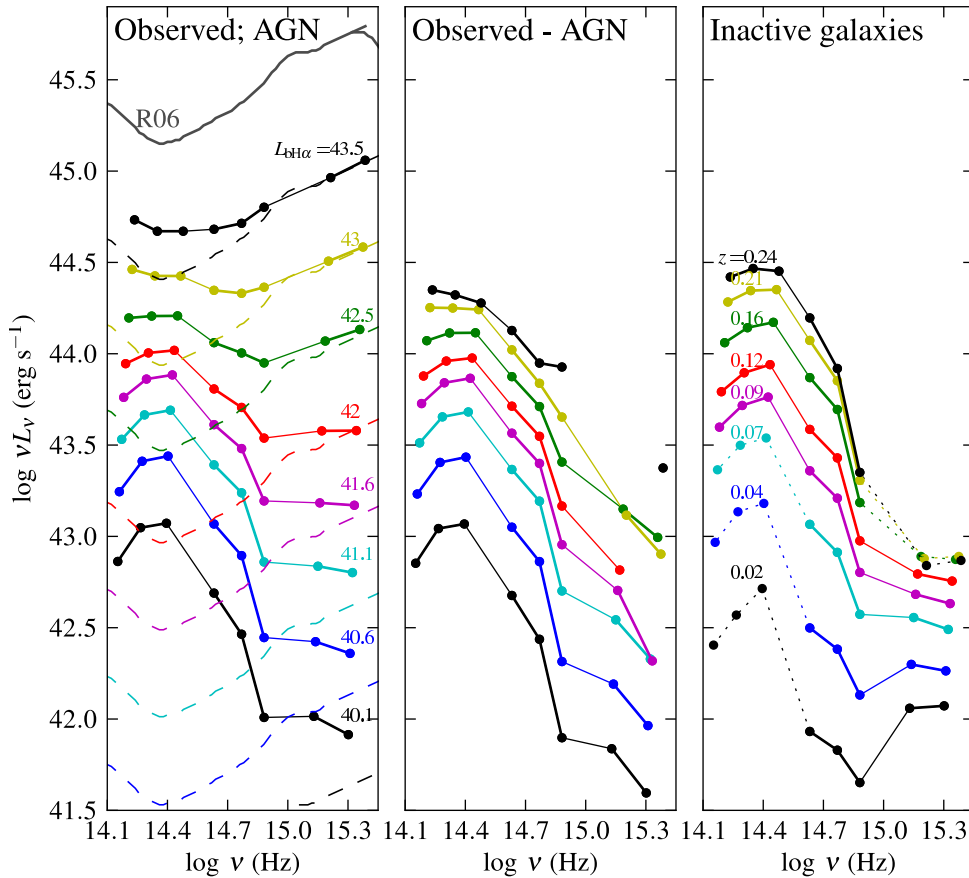


Figure 5. The luminosity dependence of the mean T1 objects SEDs at $2.2\mu\text{m} - 1528\text{\AA}$. **Left** Solid lines mark the observed SEDs for the eight $L_{\text{bH}\alpha}$ bins (mean $L_{\text{bH}\alpha}$ noted). Dashed lines mark the net AGN SED, derived by scaling the R06 quasar SED by the mean $L_{\text{bH}\alpha}$ of the bin with the same color. **Middle** Residuals of the subtraction of the the scaled R06 SEDs from the observed AGN SEDs. **Right** Mean SEDs of z -matched inactive galaxies (mean z noted). Dotted lines mark bands with $< 70\%$ detections.

(Fig. 4), which imply that the linear scaling of the net AGN SED is applicable only to the optical-UV region.

In order to quantitatively evaluate the AGN SED scaling law, we define the scaling index β , where $L_{\text{AGN}}(\lambda) \propto L_{\text{bH}\alpha}^\beta$. A β independent of wavelength λ indicates the mean AGN SED shape remains fixed with luminosity. From the qualitative analysis shown in Fig. 5, we expect $\beta \sim 1$ for λ in the optical or UV. In Figure 6, we plot the implied mean host luminosity $L_{\text{host}} \equiv \nu L_\nu - L_{\text{AGN}}$ in the SDSS u and z bands, for different $L_{\text{bH}\alpha}$ and β . As the expected mean L_{host} of a certain $L_{\text{bH}\alpha}$ bin, we use the mean luminosity of type 2 AGN with the same z distribution as the $L_{\text{bH}\alpha}$ bin. The type 2s are taken from the sample of Brinchmann et al. (2004).

The top panel of Fig. 6 shows that in the u band, $\beta < 0.9$ is ruled out, as the implied residual is negative for $L_{\text{bH}\alpha} > 10^{41} \text{ erg s}^{-1}$. It is remarkable that the simplest scaling, $\beta = 1$ in both bands, leads to the closest match of the mean type 1 host to the mean type 2 host. Together with the linear $\nu L_\nu(\text{UV}) - L_{\text{bH}\alpha}$ relationship at high luminosities (Fig. 4), this implies that the mean optical-UV net AGN SED has a fixed shape, and scales linearly with $L_{\text{bH}\alpha}$.

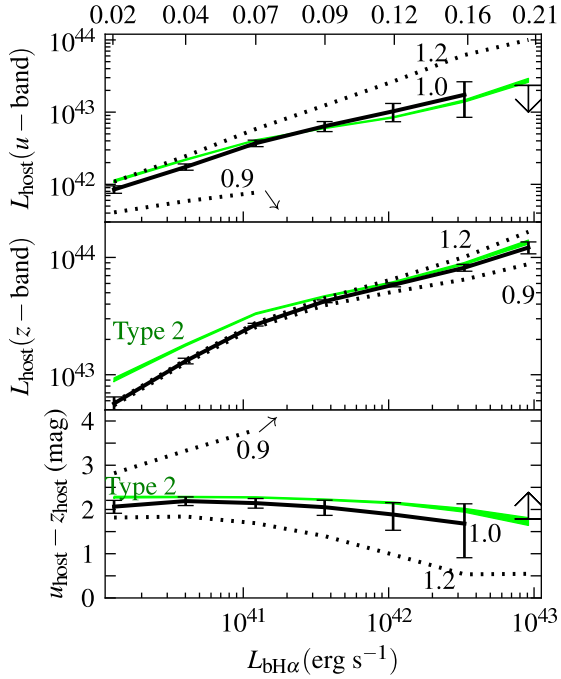


Figure 6. A comparison of the implied mean T1 host luminosity for different $L_{\text{bH}\alpha}$ bins, for different AGN SED scaling laws (black solid/dotted lines, β noted), with z -matched type 2 AGN. The comparison is made in the u band (3551\AA), z band (8932\AA), and $u - z$ color. The mean z of each $L_{\text{bH}\alpha}$ bin is noted on top. Arrows mark a negative implied host.

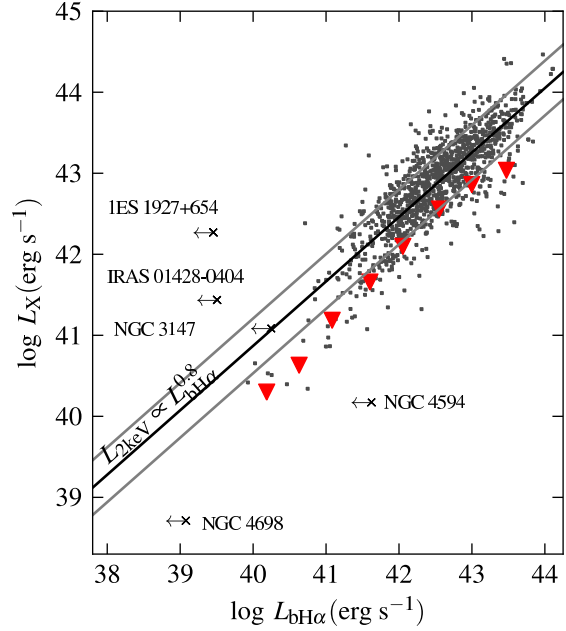


Figure 7. The L_X vs. $L_{\text{bH}\alpha}$ relation, as a probe of true type 2 AGN. Dots mark T1 objects with $F_{\text{bH}\alpha} > 10^{-13.5} \text{ erg s}^{-1} \text{ cm}^{-2}$. Red triangles mark mean upper limits in 0.5-dec $L_{\text{bH}\alpha}$ bins. The best power law fit and dispersion are shown as black and gray lines (slope noted). Arrows mark the upper limits on $L_{\text{bH}\alpha}$ of five true type 2 candidates.

6. Is the lack of BLR emission in true type 2 candidates significant?

True type 2 candidates are AGN in which the BLR is not observed, despite apparently unobscured X-ray emission. In Figure 7 we compare the upper limits on $L_{\text{bH}\alpha}$ in five true type 2 candidates from Shi et al. (2010) and Tran et al. (2011), with the T1 sample $L_X (\equiv \nu L_\nu(2\text{keV}))$ vs. $L_{\text{bH}\alpha}$ relation. Upper limits on $L_{\text{bH}\alpha}$ are derived from the expected Δv (based on the published M_{BH} and L/L_{Edd} , §3) and the flux density near $\text{H}\alpha$. The absence of a broad $\text{H}\alpha$ in NGC 4594, NGC 4698, and NGC 3147 is not significant. In the other two objects the expected $L_{\text{bH}\alpha}$ is well above the upper limits, and these two objects appear to be true type 2 AGN.

7. What drives the dispersion in the optical-UV SED of AGN?

In §5 we have shown that the mean SED of broad line AGN is well reproduced by the sum of the mean SED of luminous quasars, scaled down by $L_{\text{bH}\alpha}$, and a host contribution. Here, we examine the dispersion in the shapes of individual SEDs.

In Figure 8, we show the distributions of $\nu L_\nu(\text{FUV})/L_{\text{bH}\alpha}$ and optical slope α_{opt} as a function of $L_{\text{bH}\alpha}$. The $\nu L_\nu(\text{FUV})/L_{\text{bH}\alpha}$ distributions for $\log L_{\text{bH}\alpha} > 40.5$ have a very similar shape. All distributions have a narrow peak, with an extended tail towards low $\nu L_\nu(\text{FUV})/L_{\text{bH}\alpha}$ values. The narrow peak suggests there is a small dispersion in the covering factor of the BLR. In the $\log L_{\text{bH}\alpha} = 40.5$ bin, host contribution to the UV broadens the distribution and increases the mean value.

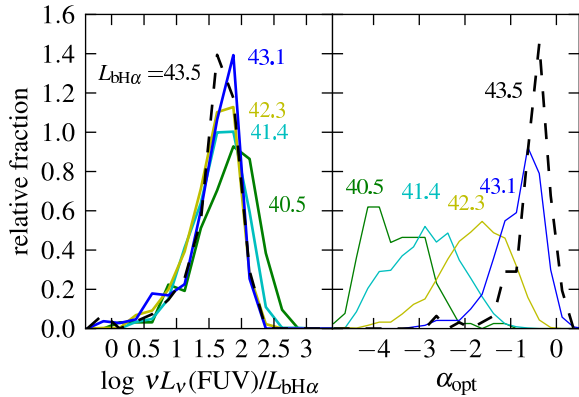


Figure 8. The T1 objects $\nu L_\nu(\text{FUV})/L_{\text{bH}\alpha}$ and α_{opt} distributions as a function of $L_{\text{bH}\alpha}$. Solid (dashed) lines represent bins of width 1 (0.5) dec in $L_{\text{bH}\alpha}$. The mean $L_{\text{bH}\alpha}$ are noted.

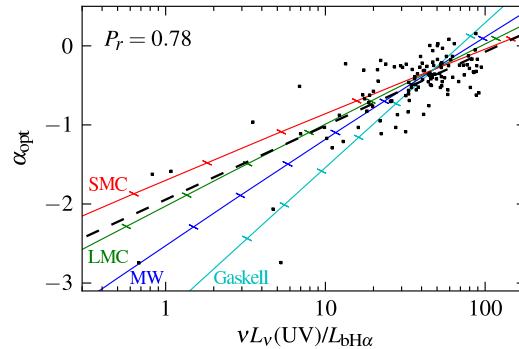


Figure 9. The α_{opt} vs. $\nu L_\nu(\text{UV})/L_{\text{bH}\alpha}$ of the T1 objects in the $\log L_{\text{bH}\alpha} = 43.5$ bin. Also shown are the best fit (dashed line) and expected relations for different extinction laws (solid lines, marks every 0.1 in $E_{\text{B}-\text{V}}$).

The α_{opt} distributions are redder at lower luminosities, due to the host emission. The $\log L_{\text{bH}\alpha} = 43.5$ bin is least affected by the host contribution, and has a narrow peak and extended red tail, similar to the $\nu L_\nu(\text{FUV})/L_{\text{bH}\alpha}$ distribution, and to the continuum slope distribution found by Richards et al. (2003) on luminous quasars. There is therefore a small dispersion in $\nu L_\nu(\text{FUV})/L_{\text{bH}\alpha}$ and α_{opt} in the net AGN emission, based on the objects least affected by the host contribution. The similar shape may indicate a common origin of the dispersion, such as dust reddening.

The dust reddening scenario is explored in Figures 9 and 10. In Fig. 9 we plot α_{opt} vs. $\nu L_\nu(\text{FUV})/L_{\text{bH}\alpha}$ for the $\log L_{\text{bH}\alpha} = 43.5$ bin. The two independent ratios are highly correlated, as expected if dust extinction contributes to the dispersion of the AGN SED. An SMC/LMC extinction law (using the Pei 1992 formulation) is preferred over a Milky Way or Gaskell & Benker (2007) extinction law, as found by Hopkins et al. (2004) on luminous quasars. In Fig. 10, we plot the $2.2 \mu\text{m} - 2 \text{keV}$ mean SED for different α_{opt} bins at the highest $L_{\text{bH}\alpha}$ bins. In the $\log L_{\text{bH}\alpha} = 43.5$ panel, the difference between SEDs increases from the NIR to the UV and disappears in the X-ray, also consistent with dust extinction. A similar behavior is observed in the $\log L_{\text{bH}\alpha} = 43$ panel, together with a weak anti-correlation of NIR luminosity and α_{opt} . The latter trend originates from the range of host luminosities, where a relatively luminous host increases $\nu L_\nu(1.2 \mu\text{m})$ and decreases α_{opt} .

The reddening origin for the dispersion in the net AGN SED implied by Figs. 9 and 10, already at $\alpha_{\text{opt}} > -1$, indicates that the intrinsic AGN SED dispersion is even smaller than seen in Fig. 8. A rather uniform and blue intrinsic optical-UV SED is expected if AGN are powered by a thin accretion disc, which emits locally close to a blackbody.

8. Conclusions

We present and analyze a new sample (T1) of 3579 broad H α selected AGN from the SDSS DR7, with $\log L_{\text{bH}\alpha} = 40 - 44$, which spans $m = 6 - 9$ and $l = -3 - 0$. We add UV (GALEX), IR (2MASS), and X-ray (ROSAT) luminosities to form the mean SED. The main results are:

- (i) The H α FWHM velocity distribution $dN/d \log \Delta v$ is independent of luminosity and falls exponentially with Δv . The origin of this distribution remains to be understood.
- (ii) The observed mean $9000\text{\AA} - 1500\text{\AA}$ SED, as a function of $L_{\text{bH}\alpha}$, is consistent with a sum of the mean SED of luminous quasars, which scales linearly with $L_{\text{bH}\alpha}$, and a host galaxy

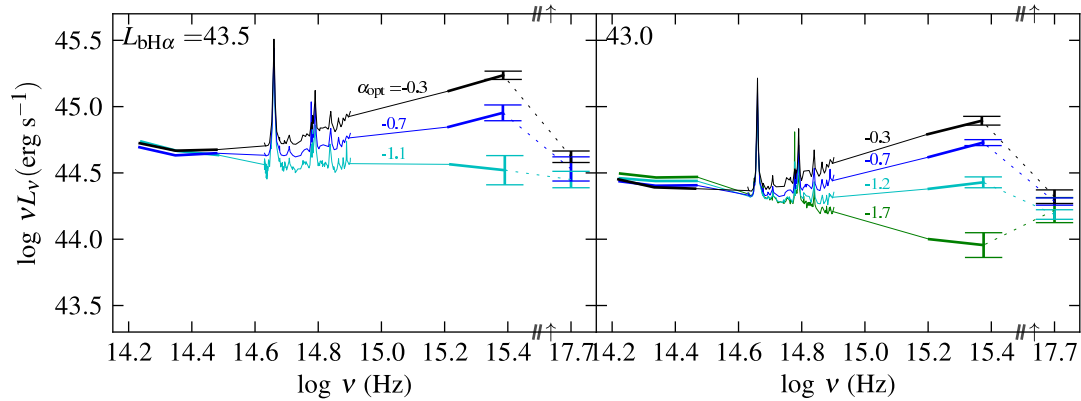


Figure 10. The mean IR to X-ray SEDs and optical spectra as a function of α_{opt} , for T1 objects with $L_{\text{bH}\alpha} = 10^{43.5}$ and 10^{43} erg s^{-1} . The value of L_X is shifted upward (+1 dec) for presentation. The error bars denote the errors in the mean L_X and $\nu L_\nu(\text{FUV})$.

contribution.

- (iii) The host galaxy r -band luminosity function of T1 objects follows the NEG luminosity function, with a relative normalization of $\sim 3\%$, suggesting that the host of broad line AGN are NEG, and the AGN probability of occurrence is independent of the host mass.
- (iv) The dispersion in the optical-UV SED in luminous AGN ($\log L_{\text{bH}\alpha} \geq 43$), is consistent with reddening. This indicates the intrinsic SED of AGN is blue, with a small dispersion, as predicted from thermal thin accretion disc models.
- (v) The $L_{\text{bH}\alpha}$ versus L_X correlation provides a useful probe for unobscured narrow line AGN. It can be used to test if the absence of a broad $\text{H}\alpha$, in X-ray detected AGN, is significant.

References

- Abazajian K N *et al* 2009 *ApJS* **182** 543
 Brinchmann J, Charlot S, White S D M, Tremonti C, Kauffmann G, Heckman T and Brinkmann J 2004 *MNRAS* **351** 1151
 Elitzur M and Shlosman I 2006 *ApJ* **648** L101
 Fine S *et al* 2008 *MNRAS* **390** 1413
 Fine S *et al* 2010 *MNRAS* **409** 591
 Gaskell C M and Benker A J 2007 *ArXiv e-prints* 0711.1013
 Greene J E and Ho L C 2005 *ApJ* **630** 122
 Hopkins P F *et al* 2004 *AJ* **128** 1112
 Kauffmann G *et al* 2003 *MNRAS* **346** 1055
 Laor A and Davis S W 2011 *MNRAS* **417** 681
 Martin D C *et al* 2005 *ApJ* **619** L1
 Nicastro F 2000 *ApJ* **530** L65
 Pei Y C 1992 *ApJ* **395** 130
 Richards G T *et al* 2003 *AJ* **126** 1131
 Richards G T *et al* 2006 *ApJS* **166** 470 (R06)
 Schneider D P *et al* 2010 *AJ* **139** 2360
 Shen Y, Greene J E, Strauss M A, Richards G T and Schneider D P 2008 *ApJ* **680** 169
 Shi Y, Rieke G H, Smith P, Rigby J, Hines D, Donley J, Schmidt G and Diamond-Stanic A M 2010 *ApJ* **714** 115
 Skrutskie M F *et al* 2006 *AJ* **131** 1163
 Stern J and Laor A, accepted for publication in *MNRAS*, *ArXiv e-prints* 1203.3158
 Tran H D, Lyke J E and Mader J A 2011 *ApJ* **726** L21
 Voges W *et al* 1999 *A&A* **349** 389
 Zheng W, Kriss G A, Telfer R C, Grimes J P and Davidsen A F 1997 *ApJ* **475** 469